*Anal. Chem.* **1996,** *68,* 3534−3538

# Single-Measurement Excitation/Emission Matrix Spectrofluorometer for Determination of Hydrocarbons in Ocean Water. 1. Instrumentation and Background Correction

Allen R. Muroski, Karl S. Booksh,† and M. L. Myrick*

*Department of Chemistry and Biochemistry, University of South Carolina, Columbia, South Carolina 29208*

**A spectrofluorometer capable of dispersed-spectrum, simultaneous, multiwavelength UV excitation and collection of luminescence has been constructed for the purpose of qualitatively and quantitatively determining aromatic hydrocarbon pollutants dissolved in ocean water. Hydrocarbon fluorescence data produced by this instrument were in the form of excitation/emission matrices, which provide more spectral information about these complex mixtures than is available from conventional excitation or emission fluorescence profiles. Second-order statistical methods were applied to these data to determine low part-per-billion concentrations of two primary fluorescent compounds, naphthalene and styrene, found in ocean water exposed to gasoline despite the presence of uncalibrated interference from similar aromatic compounds, the ocean water matrix, and the instrumental background.**

Hydrocarbon pollutants enter the aqueous environment from many sources, including industrial effluents, municipal waste discharges, atmospheric fallout, and accidental and intentional spills. The increasingly ubiquitous presence of hydrocarbons, such as those derived from petroleum, in oceans, lakes, and rivers necessitates the development of practical means for determining such pollutants in natural waters.

Petroleum products, such as gasolines and crude oils, contain a large number of compounds of varying characteristics, and the exact composition of any given mixture of these hydrocarbons varies with its source.[1] Upon exposure to water, certain components of petroleum are extracted by the aqueous phase. This partitioning occurs more rapidly and extensively in the case of the more hydrophilic compounds in the hydrocarbon mixture, such that the concentrations of particular hydrocarbons in the aqueous phase differ from those in the oil from which these compounds originate.[1] Nonetheless, identification of the source of hydrocarbon contamination is possible based on the composition of the aqueous phase.

The determination of the individual components comprising such a complex mixture is feasible using the combined techniques of gas or liquid chromatography and mass spectrometry;[2] however, the time and sample preparation necessary for a chromatographic separation make GC/MS and LC/MS ill-suited to real-time analyses. Optical techniques, such as absorbance and luminescence spectroscopy, are better-suited to rapid data collection with minimal sample pretreatment.

Fluorometry, in particular, has been applied to oil spill investigations,[3,4] determinations of petroleum residues in seawater,[5,6] and studies of the uptake of hydrocarbons in marine organisms[7] by virtue of its high sensitivity and selectivity with respect to the aromatic content of complex hydrocarbon mixtures. This aromatic fraction is of particular interest because of its toxic nature and its stability toward environmental weathering.

A conventional fluorescence spectrum is either a plot of luminescence intensity at a fixed emission wavelength as a function of excitation wavelength (an excitation spectrum) or a plot of luminescence intensity at a single excitation wavelength as a function of emission wavelength (an emission spectrum). The fluorescence of a complex mixture of fluorophores can be represented as a two-dimensional matrix of fluorescence intensity as a function of both excitation and emission wavelength. Cross sections of this excitation/emission matrix (EEM) at fixed excitation wavelengths and at fixed emission wavelengths are, respectively, standard emission and excitation spectra.

Excitation or emission spectra alone do not contain sufficient information to differentiate hydrocarbon mixtures of similar composition.[3] This deficiency exists because, among closely related compounds, excitation and emission profiles are very similar and are broad and structureless for many species in aqueous solution. It has been demonstrated, however, that EEM spectroscopy can be successfully applied to real oil spills (crude oils, fuel oils, and bilge water discharges), allowing the matching of a contaminant to its source.[3,4]

EEMs are typically generated by scanning a monochromator to produce an emission spectrum while another monochromator scans the excitation wavelength incrementally.[8] Another type of EEM system uses a spectrograph to capture emission spectra but still requires a means of scanning excitation energy.[9] Among the

† Present address: Department of Chemistry and Biochemistry, Arizona State University, Tempe, AZ 85287.

(1) Neff, J. M. *Chem. Eng. Prog.* **1987**, *83*, 27−33.
(2) Wang, Z.; Fingas, M. *LC-GC* **1995**, *13*, 950−958.
(3) Grigson, S. J.; Scotland, W. R.; Soutar, I. *Anal. Proc. (London)* **1985**, *22*, 266−268.
(4) Soutar, I. *Anal. Proc. (London)* **1983**, *20*, 19−21.
(5) Bidleman, T. F.; Castleberry, A. A.; Foreman, W. T.; Zaranski, M. T.; Wall, D. W. *Estuarine Coastal Shelf Sci.* **1990**, *30*, 91−109.
(6) Coble, P. G.; Green, S. A.; Blough, N. V.; Gagosian, R. B. *Nature* **1990**, *348*, 432−435.
(7) Jackson, L. F.; Bidleman, T. F. *Oil Chem. Pollut.* **1990**, *6*, 1−19.
(8) Ingle, J. D.; Crouch, S. R. *Spectrochemical Analysis*; Prentice Hall: Englewood Cliffs, NJ, 1988; p 445.
(9) Desiderio, R. A.; Cowles, T. J.; Moum, J. N.; Myrick, M. L. *J. Atmos. Ocean. Technol.* **1993**, *10*, 209−224.



S0003-2700(96)00252-1 CCC: $12.00 

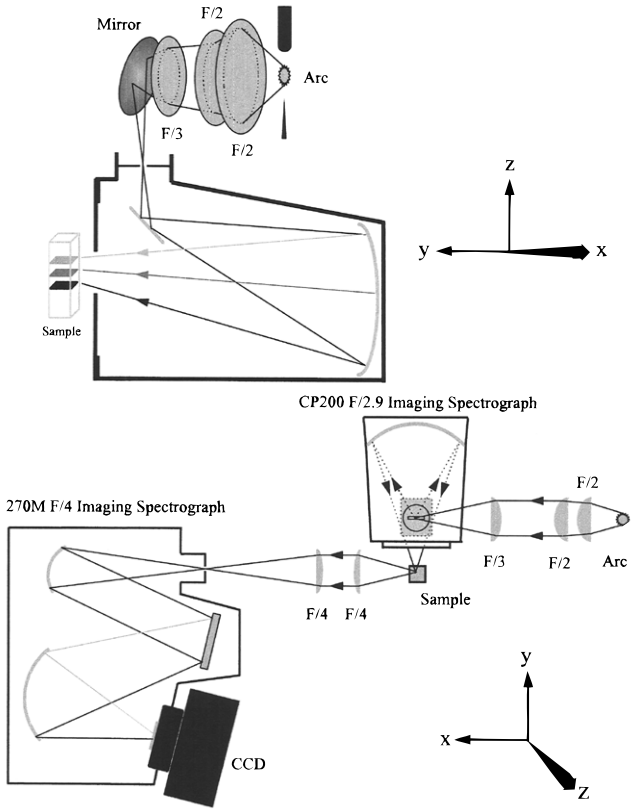


Figure 1. (a, top) Side view schematic of the imaging spectrofluorometer illustrating the spatial relationship between the excitation optics and the sample. (b, bottom) Top view schematic of the imaging spectrofluorometer illustrating the spatial relationship between the excitation optics and the emission optics.

disadvantages of these collection schemes are the extended time required for scanning and the limited wavelength reproducibility resulting from finite tolerances in the moving parts of the scanning mechanism. Additionally, different elements in an EEM produced by a scanning system are collected at different points in time and thus effectively represent different samples if the sample matrix changes during the data acquisition period. By contrast, spectrofluorometers similar to the instrument described herein have been constructed using imaging wavelength selection devices to achieve simultaneous time integration of fluorescence at all wavelengths in the EEM.[10] The objective of this paper is to describe the combination of an EEM spectrofluorometer with multidimensional data analysis as a means of producing practical EEM fluorescence information at a rate much faster than that available from other systems.

## INSTRUMENTAL SECTION

Figure 1 shows the schematics of the imaging spectrofluorometer. Figure 1a illustrates the spatial relationship between the condensing optics of the lamp and the excitation spectrograph. Figure 1b is a top view of the complete instrument with the exception of the mirror, above the entrance slit of the excitation spectrograph, which has been omitted for clarity. UV excitation was provided by an Oriel Model 66021 high-pressure 1000-W Hg-(Xe) short-arc lamp with a synthetic fused-silica envelope. This light source produced broad and intense Hg emission lines within the range of 250−600 nm which augmented the continuum output (300−800 nm) of the Xenon fill gas. Radiation from the arc was collected by a two-element condenser, focused by an F/3 lens, and reflected 90° by a plane mirror onto the entrance slit of an ISA/Jobin-Yvon Model CP200 F/2.9, 0.190 m imaging spectrograph. The dispersive element of the CP200 was a concave holographic grating with 200 grooves/mm having a groove modulation suitable for use in the ultraviolet. This combination produced a linear dispersion of 25.2 nm/mm in its focal plane. A spatial filter was used for rejection of excitation radiation other than ultraviolet light in the first grating order. The spectrograph was turned 90° onto its side, such that the source was dispersed vertically instead of horizontally. This arrangement directed shorter wavelengths nearer the top of a cuvette positioned such that the focal plane of the CP200 was located at one of the corners (upper left with reference to Figure 1b) of the cuvette, minimizing the distances traversed through the sample by the excitation radiation to its focus and by the fluorescence along the collection axis. The center of the excitation wavelength interval could be shifted by raising or lowering the entire spectrograph, which was mounted on a vertical translation stage for this purpose.

Fluorescence from the sample was collected and collimated at 90° with respect to the excitation axis by an F/4 plano-convex lens and then focused at the slit of a second imaging spectrograph by another identical lens; the collection axis was aligned in the excitation focal plane. The emission wavelength sorter was a Spex Model 270M 0.270-m, F/4 Czerny/Turner configuration device utilizing a ruled plane grating with 300 grooves/mm, blazed at 300 nm. The grating was mounted on a turret which, through its rotation, allowed for selection of the center of the emission wavelength interval. All refractive optics in the instrument were made of UV-grade synthetic fused silica. Collection of fluorescence using these chromatic lens elements limits the range of wavelengths within the EEM over which a satisfactory focus can be simultaneously obtained. This limitation exists because the dispersion by the lens material increases rapidly with decreasing ultraviolet wavelength. The use of reflective, instead of refractive, optics would eliminate this aberration; however, these were not implemented during this work.

Signal detection was via a Santa Barbara Instrument Group Model ST-6 thermoelectrically cooled CCD camera.[11] The active area of the Texas Instruments TC241 CCD used in the ST-6 is 8.6 mm wide and 6.5 mm high containing 750 × 242 pixels, each of which is 11.5 $\mu$m × 27 $\mu$m in area. The camera housing had been modified for enhanced UV throughput by removing a protective glass cover from the array and by replacing the 2.5-cm-diameter glass window with one made of synthetic fused silica. A water jacket constructed from copper tubing had also been fitted to the housing of the CCD in order to improve heat flow from the normally air-cooled sinks in thermal contact with the TEC. This latter modification allowed the array to be operated at a minimum of −42 °C, using a pump to circulate water from an ice bath through the jacket. The active area of the CCD and the linear dispersions of the spectrographs combined to produce an EEM which covered approximately 115 nm in the excitation space and 105 nm in the emission space.

(10) Warner, I. M.; Christian, G. D.; Davidson, E. R.; Callis, J. B. *Anal. Chem.* **1977**, *49*, 564−573.

(11) Cooper, J. B.; Aust, J. F.; Stellman, C.; Chike, C.; Myrick, M. L. *Spectrochim. Acta* **1994**, *50A*, 567−575.

## THEORY

With three-dimensional data structures, such as collections of EEMs, complete analyte selectivity can be achieved by mathematical separation of the analyte signal from the signal of the complex background. One method of accomplishing this separation is by employing a parallel factor analysis (PARAFAC) model to decompose the collection of EEMs into the spectral profiles of the pure component species. The PARAFAC decomposition exploits the uniqueness properties[12] intrinsic to collections of EEMs and other types of data with "bilinear" structures. An EEM of a pure compound is considered bilinear as it can be expressed as a scaled outer product of two column vectors: **x**, the excitation profile of the compound at any one emission wavelength, and **y**, the emission profile of the compound at a single excitation wavelength. That is, the EEM of a pure compound, **R**, is

$$\mathbf{R} = \hat{\mathbf{x}}\hat{\mathbf{y}}^{\mathrm{T}} + \mathbf{E} \tag{1a}$$

or equivalently

$$R_{i,j} = \hat{x}_i\hat{y}_j + E_{i,j} \tag{1b}$$

where the superscript T indicates the transpose of a matrix and the subscripts $i$ and $j$ indicate the $i$th excitation wavelength and the $j$th emission wavelength, respectively. The symbol ˆ indicates the estimate of a true spectrum, while the matrix **E** is the collection of random errors associated with any measurement. The EEM of the analyte is linear with respect to the excitation and emission profiles, hence bilinear.

In the cases of multiple fluorescent species in a sample, the bilinear model of **R** can be generalized. Here **R**, assuming linear additivity of signal, is the sum of $N$ "pure" EEMs collected at the appropriate concentrations. Hence,

$$\mathbf{R} = \sum_{n=1}^{N}\hat{\mathbf{x}}_n\hat{\mathbf{y}}_n^T + \mathbf{E} = \hat{\mathbf{X}}\hat{\mathbf{Y}}^T + \mathbf{E} \tag{2a}$$

or equivalently

$$R_{i,j} = \sum_{n=1}^{N}\hat{X}_{i,n}\hat{Y}_{j,n} + E_{i,j} \tag{2b}$$

where the $N$ columns of the matrices $\hat{\mathbf{X}}$ and $\hat{\mathbf{Y}}$, individually designated $\hat{\mathbf{x}}_n$ and $\hat{\mathbf{y}}_n$, represent the pure excitation and emission spectra of the $N$ fluorescent species in **R**. Equations 2a and 2b can be further generalized for multiple samples, $\boldsymbol{R}$, where $\boldsymbol{R}$ is an $I \times J \times K$ tensor with the index $k$ designating the sample number. The EEM of the $k$th sample in a multiple component mixture can be generalized to

$$\mathbf{R}_k = \hat{\mathbf{X}}(\hat{\mathbf{Z}}_{k,*}\mathbf{I})\hat{\mathbf{Y}}^{\mathrm{T}} + \mathbf{E}_k \tag{3a}$$

or equivalently each element in the tensor $\boldsymbol{R}$ is assumed to follow the model

$$R_{i,j,k} = \sum_{n=1}^{N}\hat{X}_{i,n}\hat{Y}_{j,n}\hat{Z}_{k,n} + E_{i,j,k} \tag{3b}$$

Here $\hat{\mathbf{Z}}$ is a $K \times N$ matrix with the $n$th column consisting of the relative concentrations of the $n$th compound throughout the $K$ samples. The subscript $k,*$ in eq 3a indicates the $k$th row, all columns, of the matrix, and **I** is the identity matrix.

The PARAFAC-based decomposition of $\boldsymbol{R}$ into estimates of the excitation and emission profiles, $\hat{\mathbf{X}}$ and $\hat{\mathbf{Y}}$, and relative concentrations, $\hat{\mathbf{Z}}$, is unique to a scalar multiple of each column in $\hat{\mathbf{Z}}$.[13] The PARAFAC decomposition can be employed to deconvolute highly overlapping spectra in EEMs collected from multiple mixtures. This permits removal of instrumental backgrounds and estimation of the number and distribution of fluorescent components in a collection of samples.[14,15]

The decomposition can be used to predict analyte concentration for unknowns when one or more samples is of known analyte concentration. Since $\hat{\mathbf{Z}}$ is unbiased by the presence of uncontrolled spectral interferents in the analytic samples, the accurate prediction of analyte concentration can be accomplished in the presence of spectral interferences that are not included in the calibration set.[15,16] This predictive asset is absent in univariate and multivariate calibration.[16] The performance of this instrument during EEM production and subsequent analysis of these EEMs by the PARAFAC model for calibration is the theme of a separate paper.[17]

## EXPERIMENTAL SECTION

A 5 mg/mL standard solution of naphthalene in ethanol was prepared by dissolving 0.500 g of scintillation-grade naphthalene crystals (99+%, Aldrich) in anhydrous ethyl alcohol (Quantum) in a 100-mL volumetric flask. A 10 parts-per-million (ppm) stock solution of naphthalene in seawater was made by adding 4.00 mL of the naphthalene/ethanol solution to ocean water rapidly stirring in a 2-L volumetric flask and then filling to the mark with ocean water. Ocean water was obtained from the Baruch Marine Science Institute, located on the north inlet of Winyah Bay near Georgetown, SC, and was not pretreated in any way. This stock solution was diluted with ocean water to produce 11 naphthalene/water standards of concentrations between 28 and 2000 parts-per-billion (ppb). A 1 ppm ($\mu$L/L) stock solution of styrene (99%, Aldrich) in ocean water was made by diluting 2 $\mu$L of styrene with the latter in a 2000-mL volumetric flask. Styrene standards ranging from 5 to 1000 ppb in ocean water were produced from this styrene stock.

EEM spectra were taken of the 11 naphthalene/ocean water standards, the styrene/ocean water standards, and several ocean water blanks using the imaging spectrofluorometer described above. The arc lamp was thermally stabilized by operation at approximately 1 kW for a minimum of 30 min before any data were collected. The CCD detector was maintained at −41 °C,

(12) Kruskal, J. D. In *Multiway Data Analysis*; Coppi, R., Bolasco, S., Eds.; Elsivier: Amsterdam, 1989.

(13) Kroonenberg, P. *Three Mode Principal Component Analysis*; DSWO Press: Leiden, The Netherlands, 1983.

(14) Ferreira, M. M. C.; Brandes, M. L.; Ferreira, I. M. C.; Booksh, K. S.; Dolowy, W. C.; Gouterman, M.; Kowalski, B. R. *Appl. Spectrosc.* **1995**, *49*, 1317−1325.

(15) Burdick, D. S.; Tu, X. M.; McGown, L. B.; Millican, D. W. *J. Chemom.* **1990**, *4*, 15−28.

(16) Booksh, K. S.; Kowalski, B. R. *Anal. Chem.* **1994**, *66*, 782A−791A.

(17) Booksh, K. S.; Muroski, A. R.; Myrick, M. L. *Anal. Chem.* **1996**, *68*, 3539−3544 (following paper in this issue).

and the entrance slit of the excitation spectrograph and that of the emission spectrograph were set at 0.25 and 0.100 mm, respectively. The emission wavelength range was centered at 340 nm for naphthalene and at 300 nm for styrene. Each standard and blank was exposed for 60 s; a "dark frame", or baseline EEM, was also collected over this time interval. Samples were contained in square cross section, UV-grade fused-silica fluorescence cuvettes of 3.5 mL internal volume. Cuvettes were flushed thoroughly with ocean water between samples and were rinsed with each sample before being filled.

**Data Pretreatment.** EEMs were collected and stored in the "low-resolution" mode (bins three pixels vertically and two pixels horizontally) of the CCD operating software in order to decrease the time required for digitization and downloading of images and to improve the signal-to-noise ratio. Each image was stored as a double-precision SBIG ASCII file.[18] These data files were then converted to double-precision ASCII files by a C++ program written in this laboratory. This conversion produced a 250 × 121 element matrix per sample. Each of these elements spanned 0.4 nm in the excitation domain and 0.9 nm in the emission domain. The actual wavelength range of each pixel varies slightly with the wavelength and center position of each spectrograph.

After conversion of the data files, each image was dark count subtracted, normalized to correct for the wavelength dependence of both the source radiance and the throughput efficiency of the excitation optics, and compressed to an 80 × 60 element matrix. All postcollection data processing was performed in the Matlab (MathWorks, Inc., Natick, MA) operating environment on Gateway P5-90 personal computers (Gateway 2000, E. Sioux Falls, SD). Data compression (3:1 em; 2:1 ex) was performed to increase data processing speed. Each element in the compressed EEM spans 1.2 nm in the excitation domain and 1.8 nm in the emission domain. This is comparable to the calculated resolution of the spectrofluorometer.

A dark frame was used to correct the EEMs for the thermal background signal from the detector. Although the dark count baseline could be incorporated in the PARAFAC model, its removal prior to lamp intensity correction is essential for determining the apparent lamp intensity profile. The lamp intensity correction was employed to permit determination of excitation profiles that are independent of the substantial variance in the radiance of the source over the range of excitation wavelengths in the EEMs. Moreover, this type of correction has the added benefit of weighting each element in the predicted excitation profiles on the basis of the relative efficiency at a particular excitation wavelength, instead of on the convolution of the fluorescence excitation efficiency and spectral irradiance of the sample. The lamp intensity profile was estimated by taking the ratio of the UV absorbance spectrum of fluorescein to that of its excitation profile as measured by the EEM spectrofluorometer. This yielded a vector of weights, the reciprocal of the lamp intensity profile, which was used to scale the *J* emission profiles in each EEM (Figure 2). No correction for the wavelength-dependent efficiencies of the detector and the collection optics or for the variation in pixel response across the detector was attempted because the effects of these on the EEMs were nominal compared to the effects of the varying spectral irradiance. It was unnecessary to produce perfectly corrected EEMs for quantitative purposes; thus, only the minimum amount of data preprocessing necessary to provide reasonable precision in the results was performed.

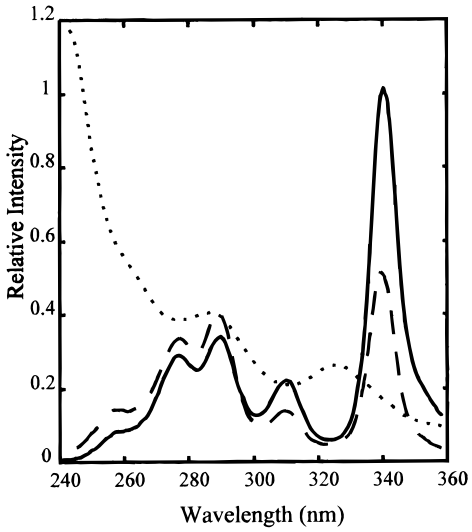


Figure 2. Estimated lamp intensity profile as a function of wavelength (solid) calculated by taking the ratio of the fluorescein fluorescence excitation profile (dashed) to that of the fluorescein absorbance spectrum (dotted).

**Profile Estimation.** The excitation/emission/concentration profiles in eqs 3a and 3b were estimated by a version of the TUCKALS3 alternating least-squares algorithm[13,19] that has been constrained to minimize the error in decomposing $\boldsymbol{R}$ based on the PARAFAC model. Termination of the alternating least-squares approximation sequence was based on the unconstrained correlation coefficient criterion.[20] Extra constraints, such as nonnegativity or unimodality, could be imposed on the estimated excitation and emission profiles; however, this was not done under the belief that the data should "speak for itself".

Two validation tools were employed to check the sufficiency of the PARAFAC decomposition to model the data. Analysis of the magnitude and distribution of the elements in the residual matrix, **E**, was first employed. When the appropriate number of factors is included in the model, inclusion of an additional factor will not significantly improve the fit of the model to the data. Similarly, when the appropriate number of factors is included in the model, the errors, **E**, should present no topological trend when plotted as an EEM. A trend would be evident if one too few factors were incorporated in the model. Finally, $\hat{\mathbf{X}}$, $\hat{\mathbf{Y}}$, and $\hat{\mathbf{Z}}$ were visually inspected to determine whether they made chemical sense.

## RESULTS AND DISCUSSION

**Instrumental Background Subtraction.** A typical spectrofluorometer minimizes stray excitation light through the use of a long-pass filter. Such a rejection element cannot effectively serve as part of a system in which broad-band excitation and emission occur simultaneously, because of the overlap of excitation radiation and fluorescence of the same wavelength. Therefore, EEMs produced by this type of instrument are characterized by a convolution of the fluorescence spectrum of the sample with a background containing, in addition to typical Stokes-shifted components, comparatively intense elastically scattered and other stray excitation radiation transmitted by the emission optics.

(18) *Software Application Note*, Santa Barbara Instrument Group, Santa Barbara, CA.

(19) Kroonenberg, P.; deLeeuw, J. *Psychometrika* **1980**, *45*, 69−97.
(20) Mitchell, B. C.; Burdick, D. S. *Chemom. Lab.* **1993**, *20*, 149−161.

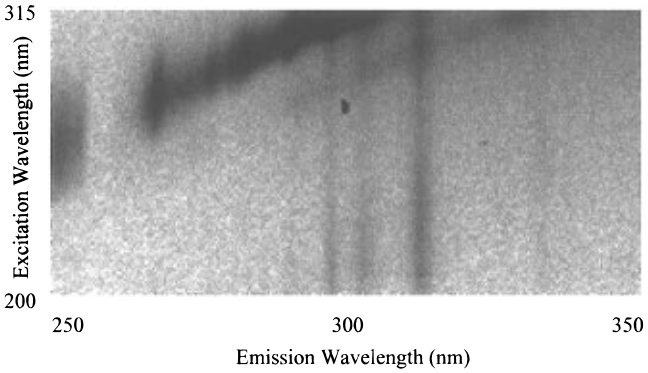


Figure 3. Untreated negative EEM image of the instrumental background measured from ocean water blank (60-s exposure).

By employing a holistic approach to the use of the imaging spectrofluorometer with multidimensional EEM deconvolution, however, the detrimental effects of a changing background signal are controlled, and the elastic-scattering component of this background can be used as an internal wavelength reference. Figure 3 shows a negative image of the background obtained using distilled water as a blank. The elastic-scattering portion of this signal manifests itself as a diagonal across the EEM corresponding to equal energy values on the excitation and emission axes. The more intense Hg lines at 254, 313, 334, and 365 nm are the most prominent features along this diagonal. Other Hg lines (e.g., 280 and 289 nm) are less intense and, therefore, not readily visible in the figure. The background is also characterized by stray light components appearing in the images as horizontal and vertical streaks. The intensities of these striations are correlated to the intensities of the lamp lines along the diagonal. This correlation supports the conclusion that these features are primarily artifacts resulting from the effects of ruled-grating imperfections on the large amount of elastically scattered excitation light entering the emission spectrograph. These scattering lines were not observed in EEMs of distilled water samples, were readily seen in those of ppb naphthalene/distilled water samples, and were very strong in EEMs of samples containing ocean water. This component of the background cannot be corrected by subtracting an instrumental blank, since the scattering is a function of the total species concentration and turbidity of the sample. Another component of the background is Raman scattering of lamp radiation by water. This scattering produces another diagonal—shifted to longer emission wavelengths compared to that produced by elastic scattering—the main features of which are Stokes-shifted Hg emission lines. These diagonals produced by elastic and inelastic scattering gradually diverge at longer wavelengths due to the constant energy difference between them.

Since the background varies among samples and is approximately bilinear, it can be successfully included in the PARAFAC model as an additional factor. The resolved profile of the background along the excitation axis has two main features; one corresponds to the elastic scattering of the 254-nm band, and the other is related to the more intense scattering of the 302-nm line. In this estimated background excitation profile the elastically scattered 302-nm line is much more intense than the other bands since the EEMs were collected near the maximum of the 302-nm line. Similarly, the resolved emission profiles have two features; the first of these corresponds to the scattered 313-nm line, the second to the 334-nm line.

Although the PARAFAC model was employed to deconvolve the scattering background from the EEMs, this model is not technically correct. The interaction of the emission- and excitation-based Rayleigh lines follows an additive model, not the multiplicative model assumed in eqs 1a and 1b. Hence, it is expected that the modeling efficiency of the background will be worse than the modeling efficiency of the naphthalene fluorescence. A plot of relative root-mean-squared error of fit (RRMSEF), where

$$\mathrm{RRMSEF} = \left(\sum_{j=1}^{J}\sum_{i=1}^{I}(\mathbf{R} - \hat{\mathbf{R}})^2\right)^{1/2} \Big/ \left(\sum_{j=1}^{J}\sum_{i=1}^{I}(\mathbf{R})^2\right)^{1/2} \quad (4)$$

for the PARAFAC model of eqs 3a and 3b versus the percent contribution of the background to the integrated fluorescence intensity allows derivation of the modeling efficiencies of the background and naphthalene. Over the range of 20% scattering background to 100% Rayleigh background, the graph is linear with a slope of 5.2% RRMSEF increase in background contribution and an intercept of −0.0019 RRMSEF; however, at less than 20% background, the RRMSEF varies around 1%. This behavior is consistent with a system where the error of fit associated with modeling the background is 5% and the error of fit associated with modeling the naphthalene fluorescence is small compared to the inherent 1% random instrumental errors.

The effects of grating imperfections are pronounced at shorter excitation wavelengths; the background fluorescence profiles and styrene fluorescence profiles could, nonetheless, be resolved from the 19 styrene/sea water mixtures. Regression of the percent background contribution against the RRMSEF yields an 18% RRMSEF associated with the background and a 5% RRMSEF associated with styrene. Nevertheless, meaningful estimates of the excitation and emission profiles were still obtained. In the estimated excitation profile, the shoulder of the intense Rayleigh region is evident between 210 and 260 nm. Also evident is a feature associated with the 280-nm lamp line. In the emission profile, the 280-, 289-, 296/302-, 313-, and 334-nm Rayleigh lines are clearly evident. It is shown in the following paper that accurate calibration was performed in spite of these small model errors associated with the background signal.

## ACKNOWLEDGMENT

The authors thank Andrew Crowson and the Army Research Office for funding (DAAH04-93-G-0324) applied to this work. K.S.B. thanks the National Science Foundation for his postdoctoral fellowship (CHE-9403179). Furthermore, the authors applaud the invaluable contribution of Michael L. McLester to the technical details of their research, and they also thank Young-Gyun Kim for his composition of the macro used to convert EEM data from its original SBIG format to the ASCII format.

Received for review March 13, 1996. Accepted June 28, 1996.[⊗]

AC960252B

[⊗] Abstract published in *Advance ACS Abstracts,* August 1, 1996.